Sparse representation of migrating targets in low PRF wideband radar

Stéphanie Bidon, Jean-Yves Tourneret, Laurent Savy

Sparse Representation of Migrating Targets in low PRF Wideband Radar

Stéphanie Bidon
Department of Electronics Optronics and Signal
ISAE, University of Toulouse
Toulouse, France
Email: sbidon@isae.fr

Jean-Yves Tourneret
IRIT - ENSEEIHT - TéSA
University of Toulouse
Toulouse, France
Email: jyt.tourneret@enseeiht.fr

Laurent Savy
Radar and Electromagnetism Department
ONERA
Palaiseau, France
Email: laurent.savy@onera.fr

***Abstract*— In wideband (high range resolution) radar, moving targets migrate along the range during the coherent processing interval (CPI). In this paper, we propose to use the information brought by this migration to alleviate the velocity ambiguity that occurs in low pulse repetition frequency (PRF) mode. More specifically, a Bayesian algorithm is implemented to give a sparse representation of the received signal while unfolding properly the range-velocity map. Though computationally intensive, the algorithm demonstrates the possibility of designing a non-ambiguous radar mode with a single PRF in case of a multi-target scenario.**

I. Introduction

For radar systems, high range resolution (HRR) is a feature in great demand as it may enhance detection of small targets in adverse environment. HRR can be achieved through the use of wideband pulse waveform [1]. However, while decreasing the range resolution cell, a phenomenon of range migration occurs for moving targets. Naturally, this migration has to be taken into account during signal processing. Despite this apparent complication, range migration can also be of great interest as it contains additional information about target velocity. If correctly processed, this information can be used to alleviate the ambiguous velocity and thus allow a non-ambiguous mode to be obtained in case of low PRF. Such possibility is investigated in this paper.

Former studies on wideband radar have shown that the target signature can be easily expressed in the fast-frequency/slow-time domain thereby leading to the definition of a coherent integration processing [2], [3]. However, sidelobes occurring at ambiguous velocities are very high and prevent from detecting multiple scatterers. Deterministic approches have been undertaken to decrease these sidelobes, e.g., in [4]. Here, we propose and study an algorithm allowing a non-ambiguous and sparse representation of the received scatterer echoes within a Bayesian framework.

The paper is organized as follows. In section II, the wideband radar data model is recalled and interpreted as the under-sampled observation of a "virtual" well-sampled signal. Section III proposes a Bayesian model appropriate to the sparse representation of this well-sampled signal. Performance of the resulting Bayesian estimators is evaluated numerically in section IV.

II. Signal model for wideband signal

A. Classical signal model

We consider in the following a radar system sending a series of M wideband pulses with a low PRF[1] $f_r = 1/T_r$. The instantaneous bandwidth B is thought to be on the order of 10% of the carrier frequency f_c. K range gates are selected for the processing. They define a low range resolution (LRR) segments containing targets of interest with allowance for range-walk.

The signature of a single point scatterer is then given in the fast-frequency/slow-time domain, for $k = 0, \ldots, K-1$ and $m = 0, \ldots, M-1$, by [3], [5]

$$[\boldsymbol{A}]_{k,m} = \exp\left\{j2\pi\left(-\tau_0\frac{B}{K}k + \frac{2vf_c}{c}T_r m\right)\right\} \quad \text{(2D-cisoid)}$$
$$\times \exp\left\{j2\pi\frac{2v}{c}\frac{B}{K}T_r km\right\} \text{ (cross-coupling terms)} \quad (1)$$

where c is the speed of light, v is the target velocity and τ_0 its initial round-trip delay. The signature (1) can be interpreted as the combination of a bi-dimensional cisoid—with frequency pair $(-\tau_0, 2vf_c/c)$ and sampling periods B/K and T_r — with cross-coupling terms that model the range migration. These terms contain information about the target velocity v in addition to the carrier Doppler frequency. Note that as an LPRF mode is assumed, the Shannon sampling theorem is not ensured for the slow-time dimension since $2v_{\max}f_c/c > 1/(2T_r)$ where $v_{\max}$ represents the maximum target velocity expected for a scatterer.

For a scenario with N_t scatterers, the whole signal can be expressed in matrix or vector[2] notation as

$$\boldsymbol{Y} = \sum_{t=1}^{N_t}\alpha_t\boldsymbol{A}_t + \boldsymbol{N} \quad \text{or} \quad \boldsymbol{y} = \sum_{t=1}^{N_t}\alpha_t\boldsymbol{a}_t + \boldsymbol{n} \quad (2)$$

where α_t and $\boldsymbol{A}_t$ designate respectively the complex amplitude and the signature (1) of the t-th scatterer and $\boldsymbol{N}$ is the $K \times M$ matrix representing the thermal noise assumed to be white

[1]Typical applications should be for instance detection of ground moving targets with an X-Band radar.

[2]Vectors here are colon-vectors obtained from the row-vectorization of their associated matrix.

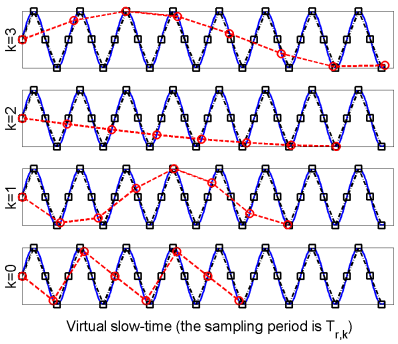

Fig. 1. Observation and resampling of a cisoid. The solid line represents the analog version of a cisoid with frequency $2vf_c/c$. The circle markers stand for the observed data with period $T_{r,k}$. The square markers stand for samples of the cisoid obtained with a thinner period $\bar{T}_r$.

from pulse to pulse and from subband to subband. (Presence of ground clutter is not investigated in this paper.)

B. Towards a sparse representation

1) Interpretation of the target signature: The signature (1) can be easily re-written as a 2D-cisoid with the same frequency pair $(-\tau_0, 2vf_c/c)$ but with a sampling period $T_{r,k}$ on the slow-time that depends on the subband index k, i.e.,

$$[\boldsymbol{A}]_{k,m} = \exp\left\{ j\ 2\pi \left(-\tau_0 \frac{B}{K} k + \frac{2vf_c}{c} T_{r,k} m \right) \right\} \quad (3)$$

where

$$T_{r,k} = (1+\mu k)\, T_r \quad \text{and} \quad \mu = B/(Kf_c).$$

The slow-time period $T_{r,k}$ increases linearly with the subband index k and a slope equal to μT_r. Since an LPRF mode is assumed, the aliasing phenomenon increases with respect to the subband index too. The concept is illustrated in Fig. 1 where the imaginary part of a 1D-cisoid with frequency $2vf_c/c$ and a sampling period $T_{r,k}$ has been represented. The cisoid is observed K times but each time with an increased sampling period. As the number of samples M remains constant regardless of the subband, the observation time of the cisoid increases with respect to the subband index k. In the following, we intend to use these K aliased observations to reconstruct the signal correctly (i.e., without velocity ambiguity).

2) Shannon reconstruction: The target component of the signal in (2) is bandlimited with respect to the slow dimension with the maximum Doppler frequency $2v_{\max}f_c/c$. Let $\bar{T}_r = 1/\bar{f}_r$ denote a sampling period that complies with the Shannon sampling theorem, i.e.,

$$\frac{2v_{\max}f_c}{c} < \frac{1}{2\bar{T}_r}.$$

The sampling theorem ensures then that, for $k = 0, \ldots, K-1$, the sequence $\{[\boldsymbol{A}]_{k,m}\}_{m=0}^{M-1}$ can be exactly reconstructed via the following interpolation formula [6]

$$[\boldsymbol{A}]_{k,m} = \sum_{\bar{m}=-\infty}^{+\infty} [\bar{\boldsymbol{A}}]_{k,\bar{m}} \mathrm{sinc}\left\{ \pi \left(m\frac{T_{r,k}}{\bar{T}_r} - \bar{m} \right) \right\}$$

where $\mathrm{sinc}(x) = \sin(x)/x$ and $\bar{\boldsymbol{A}}$ is the matrix containing the observations of the 2D-cisoid sampled at the rate $\bar{f}_r$ on the slow-time dimension, i.e.,

$$[\bar{\boldsymbol{A}}]_{k,\bar{m}} = \exp\left\{ j\ 2\pi \left(-\tau_0 \frac{B}{K} k + \frac{2vf_c}{c} \bar{T}_r \bar{m} \right) \right\}.$$

Using the linearity of the convolution operator, the received signal (2) can be re-written as follows

$$[\boldsymbol{Y}]_{k,m} = \sum_{\bar{m}=-\infty}^{+\infty} [\bar{\boldsymbol{\Lambda}}]_{k,\bar{m}} \mathrm{sinc}\left\{ \pi \left(m\frac{T_{r,k}}{\bar{T}_r} - \bar{m} \right) \right\} + [\boldsymbol{N}]_{k,m}$$

with

$$\bar{\boldsymbol{\Lambda}} = \sum_{t=1}^{N_t} \alpha_t \bar{\boldsymbol{A}}_t.$$

Note that if one could have access to $\bar{\boldsymbol{\Lambda}}$, the target peaks could be recovered via standard 2D-spectral estimators (e.g., FFT, Capon and APES filters [7], etc.). In the following, we propose to estimate the elements of $\bar{\boldsymbol{\Lambda}}$ on a certain time window $\bar{m} = 0, \ldots, \bar{M}-1$ using the following approximation

$$[\boldsymbol{Y}]_{k,m} \triangleq \sum_{\bar{m}=0}^{\bar{M}-1} [\bar{\boldsymbol{\Lambda}}]_{k,\bar{m}} \mathrm{sinc}\left\{ \pi \left(m\frac{T_{r,k}}{\bar{T}_r} - \bar{m} \right) \right\} + [\boldsymbol{N}]_{k,m}. \quad (4)$$

Note, that for the sake of simplicity, the same length $\bar{M}$ has been chosen for each subband index k. The new time sampling related to $\bar{\boldsymbol{\Lambda}}$ is represented for one cisoid with frequency $2vf_c/c$ in Fig. 1. Note that the new rate $\bar{f}_r$ allows the ambiguous velocity to be increased from $v_a = cf_r/(2f_c)$ to $\bar{v}_a = c\bar{f}_r/(2f_c)$.

For more convenience, a vectorized expression of (4) is used in the remaining of the paper. More precisely, the observed signal can be re-written as

$$\boldsymbol{y} = \boldsymbol{T}\bar{\boldsymbol{\lambda}} + \boldsymbol{n} \quad (5)$$

where $\bar{\boldsymbol{\lambda}}$ is the vector notation for $\bar{\boldsymbol{\Lambda}}$ and $\boldsymbol{T}$ is the $KM \times K\bar{M}$ block diagonal matrix built from K interpolation matrices $\boldsymbol{T}_k$ of size $M \times \bar{M}$ and defined by

$$[\boldsymbol{T}_k]_{m,\bar{m}} = \mathrm{sinc}\left\{ \pi \left[m\frac{T_{r,k}}{\bar{T}_r} - \bar{m} \right] \right\}.$$

3) Transformation to fast-time/slow-frequency domain: The vector $\bar{\boldsymbol{\lambda}}$ expressed in the fast-frequency/slow-time domain corresponds to a sum of N_t bi-dimensional cisoids. Therefore, the N_t scatterers can be ideally represented in the fast-time/slow-frequency domain by N_t peaks centered around $(-\tau_{0,t}, 2v_t f_c/c)$. To obtain a representation of the scatterer echoes as sparse as possible, the model (5) is thus finally expressed as follows

$$\boldsymbol{y} = \left[\boldsymbol{T}\boldsymbol{F}^{-1}\right]\left[\boldsymbol{F}\bar{\boldsymbol{\lambda}}\right] + \boldsymbol{n} \quad (6)$$

where $\boldsymbol{F}$ is the matrix that transforms $\bar{\boldsymbol{\lambda}}$ from the fast-frequency/slow-time domain to the fast-time/slow-frequency domain. The matrix $\boldsymbol{F}$ is given by

$$\boldsymbol{F} = \boldsymbol{F}_K^{-1} \otimes \boldsymbol{F}_{\bar{M}} \quad (7)$$

where $\otimes$ represents the Kronecker tensor product and $\boldsymbol{F}_\Delta$ is the $\Delta \times \Delta$ discrete Fourier transform matrix, i.e.,

$$[\boldsymbol{F}_\Delta]_{\delta_1,\delta_2} = \frac{1}{\sqrt{\Delta}} \exp\left\{-j2\pi \frac{\delta_1 \delta_2}{\Delta}\right\}$$

for $\delta_1, \delta_2 \in \{0, \ldots, \Delta - 1\}$. By noting

$$\boldsymbol{H} = \boldsymbol{T}\boldsymbol{F}^{-1} \quad \text{and} \quad \boldsymbol{x} = \boldsymbol{F}\bar{\boldsymbol{\lambda}} \tag{8}$$

the data model (6) can be expressed as

$$\boxed{\boldsymbol{y} = \boldsymbol{H}\boldsymbol{x} + \boldsymbol{n}.} \tag{9}$$

The matrix $\boldsymbol{F}$ in (7) represents a discrete-Fourier transform (DFT) basis. Accordingly, one can define a no basis mismatch situation when every scatterer frequency verifies: $\exists (k_t, \bar{m}_t) \in \{0, \ldots, K-1\} \times \{0, \ldots, \bar{M} - 1\}$ such that

$$\left(-\tau_t, \frac{2v_t f_c}{c}\right) = \left(\frac{-k_t}{K} \times \frac{K}{B}, \frac{\bar{m}_t}{\bar{M}} \times fs\right). \tag{10}$$

In such case, the $K\bar{M}$-length vector $\boldsymbol{x}$ defined in (8) reduces to a vector having exactly N_t non-zero elements with value $\sqrt{K\bar{M}}\alpha_t$. The vector $\boldsymbol{x}$ is thus a good candidate to produce a sparse representation of the N_t-scatterers. Observing that (9) is an ill-posed problem ($K\bar{M} \gg KM$), one could turn to well known deterministic approaches to retrieve such vector $\boldsymbol{x}$ (e.g., a quadratic program with an ℓ^1 penalty term [8]). In the following section, we rather propose to follow a Bayesian route. On one hand, prior information about the received data will be used to regularize the problem (9). On the other hand, a sparseness-promoting prior will be chosen to ensure a small amount of non-zero elements in $\boldsymbol{x}$.

III. Hierarchical Bayesian model

In this section, we describe further the data model (9) within a Bayesian framework [9] and present an associated algorithm to estimate the vector $\boldsymbol{x}$. The proposed model is an extended version of models introduced in earlier works [10]. Prior distributions are chosen to satisfy the usual compromise, i.e., expressing physical constraints while ensuring mathematical tractability. To comply with the later, priors are chosen among a family of conjugate priors. To comply with the former, they are designed to express our knowledge about the sparse-nature of the data (i.e., a finite number of scatterers), the target power and possibly the thermal noise power.

Remark 1 (Notations: vector norm): For $p \in \mathbb{N}^*$ and $\boldsymbol{x} \in \mathbb{C}^m$ the pth norm of $\boldsymbol{x}$ is defined by $\|\boldsymbol{x}\|_p = \left(\sum_{i=1}^m |x_i|^p\right)^{1/p}$. If $p = 0$, then the norm is defined as the number of nonzero vector elements, i.e., $\|\boldsymbol{x}\|_0 = \#\{i \in \{1, \ldots, m\} / x_i \neq 0\}$.

A. Bayesian data model

The hierarchical model described in this section is illustrated in Fig. 2.

1) Observation data: The white noise $\boldsymbol{n}$ is assumed to be complex Gaussian with variance σ^2, denoted by $\boldsymbol{n} \sim \mathcal{CN}_{KM}\left(\boldsymbol{0}, \sigma^2 \boldsymbol{I}\right)$. The likelihood is thus given by

$$f(\boldsymbol{y}|\boldsymbol{x}, \sigma^2) = \frac{1}{\pi^{KM}\sigma^{2KM}} \exp\left\{-\frac{\|\boldsymbol{y} - \boldsymbol{H}\boldsymbol{x}\|_2^2}{\sigma^2}\right\}. \tag{11}$$

2) Parameters:

a) Prior of σ^2: One assumes that the thermal noise power is not known and has a non-informative Jeffrey's distribution, i.e.,

$$f(\sigma^2) = \frac{1}{\sigma^2} \mathbb{I}_{[0,+\infty)}(\sigma^2) \tag{12}$$

where $\mathbb{I}_{[a,b]}$ is the indicator function defined on the interval $[a, b]$. Note that for radar applications, the thermal noise power can be often known with a good approximation [11]. Hence, the prior (12) could be easily changed to an inverse-Gamma distribution with appropriate scale and shape parameters expressing our degree of prior belief about σ^2 [12].

b) Prior of $\boldsymbol{x}$: In search of simplicity, elements of $\boldsymbol{x}$ are supposed to be independent and identically distributed (i.i.d.). The prior probability density function (PDF) for each element $x_i = [\boldsymbol{x}]_i$ is then chosen to ensure a certain level of sparsity. To do so, we consider a mixed type distribution which is similar to the one investigated in [10] for sparse image recovery. More precisely, we assign a probability $(1 - w)$ that x_i is exactly equal to zero and a probability w that x_i is Gaussian with zero mean and variance σ_x^2, i.e., for $i = 1, \ldots, K\bar{M}$

$$f(x_i|w, \sigma_x^2) = (1 - w)\, \delta(|x_i|) + w\, \frac{1}{\pi\sigma_x^2} \exp\left\{-\frac{|x_i|^2}{\sigma_x^2}\right\}.$$

As the x_i's are i.i.d., the prior distribution of $\boldsymbol{x}$ is given by

$$f(\boldsymbol{x}|w, \sigma_x^2) = (1 - w)^{n_0} \left(\frac{w}{\pi\sigma_x^2}\right)^{n_1} \operatorname{etr}\left\{-\frac{\|\boldsymbol{x}\|_2^2}{\sigma_x^2}\right\} \prod_{i/x_i=0} \delta(|x_i|) \tag{13}$$

where $\operatorname{etr}\{\}$ is the exponential of the trace of the matrix between braces and

$$n_1 = \|\boldsymbol{x}\|_0 \quad \text{and} \quad n_0 = K\bar{M} - \|\boldsymbol{x}\|_0. \tag{14}$$

The PDF (13) depends on two hyperparameters w and σ_x^2 that are not exactly known *a priori*. We thus introduce another hierarchical level in the Bayesian model and describe hereafter the prior distributions chosen for these two hyperparameters.

3) Hyperparameters:

a) Prior of w: According to (13), the weight w controls the level of sparsity in the vector $\boldsymbol{x}$. Within this work, we do not favor any particular level of sparsity and assume a non-informative uniform prior for w, denoted as $w \sim \mathcal{U}_{[0,1]}$, i.e.,

$$f(w) = \mathbb{I}_{[0,1]}(w). \tag{15}$$

b) Prior of σ_x^2: According to (13), the hyperparameter σ_x^2 represents the power of each non-zero element of $\boldsymbol{x}$, i.e.,

$$\mathcal{E}\left\{|x_i|^2 | x_i \neq 0\right\} = \sigma_x^2. \tag{16}$$

Moreover, in case of no basis mismatch (10), one has

$$\mathcal{E}\left\{|x_i|^2 | x_i \neq 0\right\} = K\bar{M} \times \mathcal{E}\left\{|\alpha_t|^2\right\}. \tag{17}$$

Expressions (16) and (17) show that σ_x^2 is directly related to the power of the scatterers echoes that can be approximately predicted by the radar equation [11]. To ensure mathematical

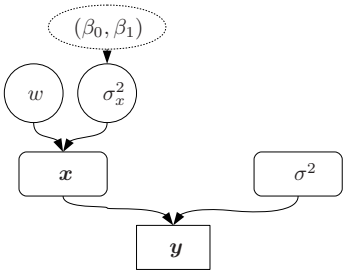

Fig. 2. Graphical representation of the proposed Bayesian model.

tractability, an inverse-Gamma PDF is chosen with shape and scale parameters (β_0, β_1). This distribution is denoted hereafter by $\sigma_x^2|\beta_0, \beta_1 \sim \mathcal{IG}(\beta_0, \beta_1)$ and is such that

$$f(\sigma_x^2|\beta_0, \beta_1) \propto \frac{e^{-\beta_1/\sigma_x^2}}{\sigma_x^{2(\beta_0+1)}} \mathbb{I}_{[0,+\infty)}(\sigma_x^2) \tag{18}$$

where $\propto$ means "proportional to". Mean and variance for $\mathcal{IG}(\beta_0, \beta_1)$ are given, when they exist, by

$$\mathcal{E}\left\{\sigma_x^2|\beta_0, \beta_1\right\} = \frac{\beta_1}{\beta_0 - 1} \quad (\beta_0 > 1) \tag{19a}$$

$$\text{var}\left\{\sigma_x^2|\beta_0, \beta_1\right\} = \frac{\beta_1^2}{(\beta_0 - 1)^2(\beta_0 - 2)} \quad (\beta_0 > 2). \tag{19b}$$

Numerical values for (β_0, β_1) can be chosen to obtain a prior either tightly clustered around its mean or diffuse when the prior belief about the target power becomes low. For instance, when $\beta_0, \beta_1 \to 0$ a flat prior is obtained, e.g., $\mathcal{IG}\left(10^{-10}, 10^{-10}\right)$ [12]. As seen later in Section IV, we have rather considered values that lead to a moderately-informative prior where σ_x^2 has well-defined mean and variance (19).

B. Bayesian estimation

From now on, our goal is to estimate the random vector $\boldsymbol{x}$ of length $K\bar{M}$ given the observation $\boldsymbol{y}$ and the hierarchical Bayesian model represented in Fig. 2 and defined by (9), (11), (12), (13), (15) and (18). We recall that the known quantities[3] of this model are

$\boldsymbol{y}$	the observed data
$\boldsymbol{H}$	the interpolation-transform matrix
(β_0, β_1)	parameters set by the operator

while $\boldsymbol{x}, \sigma^2, w, \sigma_x^2$ are unknown and need to be estimated. Common Bayesian estimators are the minimum mean square error (MMSE) and the maximum *a posteriori* (MAP) estimators [9], [13]. They are respectively defined as the mean of the posterior distribution and the argument that maximizes this former. For the parameter of interest $\boldsymbol{x}$, they are thus defined as follows

$$\hat{\boldsymbol{x}}_{\text{MMSE}} = \int \boldsymbol{x} f(\boldsymbol{x}|\boldsymbol{y}) d\boldsymbol{x} \tag{20a}$$

$$\hat{\boldsymbol{x}}_{\text{MAP}} = \arg\max_{\boldsymbol{x}} f(\boldsymbol{x}|\boldsymbol{y}). \tag{20b}$$

[3]For the sake of convenience, constant and known terms (aside the observed data $\boldsymbol{y}$) are omitted in the conditional terms.

Both rely on the posterior distribution $f(\boldsymbol{x}|\boldsymbol{y})$ that is given, according to our hierarchical model, by

$$\boxed{f(\boldsymbol{x}|\boldsymbol{y}) \propto \frac{B(1+n_1, 1+n_0)\,\Gamma(\beta_0+n_1)}{(\beta_1 + \|\boldsymbol{x}\|_2^2)^{\beta_0+n_1}\,\|\boldsymbol{y} - \boldsymbol{H}\boldsymbol{x}\|_2^{2KM}} \prod_{i/x_i=0} \delta(|x_i|)} \tag{21}$$

where $B(.)$ and $\Gamma()$ are the Beta and Gamma functions respectively. Observing (21) and recalling that n_0 and n_1 depends on $\boldsymbol{x}$ via (14), it is to our knowledge not possible to derive in closed form either the MMSE or the MAP estimator of $\boldsymbol{x}$. We propose instead to obtain them via numerical simulations by implementing a Monte-Carlo Markov chain (MCMC). Such chain generates, after an appropriate number of iterations N_{bi}, samples $(\sigma^{2(m_c)}, w^{(m_c)}, \boldsymbol{x}^{(m_c)}, \sigma_x^{2(m_c)})$ that are distributed according to the joint posterior PDF $f(\boldsymbol{x}, \sigma^2, w, \sigma_x^2|\boldsymbol{y})$. It has also the property to have each of its subsequence[4] $(\theta^{(m_c)})$ asymptotically distributed according to the posterior PDF $f(\theta|\boldsymbol{y})$. Therefore, empirical estimators of $\boldsymbol{x}$ can be obtained in the following way

$$\hat{\boldsymbol{x}}_{\text{MMSE}} \triangleq \frac{1}{N_r} \sum_{m_c=1}^{N_r} \boldsymbol{x}^{(m_c+N_{bi})} \tag{22a}$$

$$\hat{\boldsymbol{x}}_{\text{MAP}} \triangleq \arg \max_{\{\theta^{(m_c+N_{bi})}\}_{m_c=1}^{N_r}} f(\boldsymbol{x}^{(m_c)}|\boldsymbol{y}) \tag{22b}$$

where N_r is the number of samples required to approximate correctly the MMSE estimator. In this work, the implemented MCMC method is a multi-stage Gibbs sampler [13] consisting of four main iterative steps where for each parameter a sample is drawn according to its conditional posterior distribution. These four moves are built according to the joint posterior PDF given by (details can be found in [14])

$$\begin{aligned} f(\sigma^2, w, \boldsymbol{x}, \sigma_x^2, |\boldsymbol{y}) \propto\ & f(\boldsymbol{y}|\boldsymbol{x}, \sigma^2) \\ & \times f(\boldsymbol{x}|w, \sigma_x^2) f(\sigma_x^2) f(w) f(\sigma^2). \end{aligned} \tag{23}$$

IV. Numerical simulations

A. Simulation scenario

Radar data to be processed are generated synthetically according to the model described by (2). $N_t = 7$ scatterers are generated *without basis mismatch* (10). These scatterers correspond to three targets distant from one or two ambiguous velocities. Two of these targets are extended in range. The signal-to-noise ratio (SNR) for the t-th scatterer is defined as

$$SNR_t = \mathcal{E}\left\{|\alpha_t|^2\right\} \|\boldsymbol{a}_t\|_2^2 \times \left[KM\sigma^2\right]^{-1}.$$

SNRs and positions of the scatterers are depicted in Fig. 3(a). Also, for each scatterer the argument of the amplitude is drawn randomly on $[0, 2\pi[$. Other scenario and processing parameters are depicted in Tables I and II. Note that a scatterer with velocity $v_a = 15$ m/s would migrate of 6.4 range gates during the CPI while the range resolution is equal to $c/(2B) = 15$ cm.

[4]The notation θ designates successively σ^2, w, σ_x^2 and $\boldsymbol{x}$.

TABLE I

SCENARIO PARAMETERS

carrier	$f_c = 10$ GHz
bandwidth	$B = 1$ GHz
PRF	$f_r = 1$ kHz
# pulses	$M = 64$
LRR segment	$K = 8$
noise power	$\sigma^2 = 1$

TABLE II

PROCESSING PARAMETERS

σ_x^2 prior	$(\beta_0, \beta_1) \approx (28, 7.2e4)$
virtual PRF	$f_r \approx 4.67$ kHz
virtual # pulses	$\bar{M} = 329$
burn-in	$N_{bi} = 500$
Gibbs-iterations	$N_r = 2e3$

Also, the virtual PRF has been multiplied by a factor ≈ 5 so that the new ambiguous velocity is $\bar{v}_a \approx 70$ m/s. Finally, the hyperparameters (β_0, β_1) that define the prior for σ_x^2 have been chosen according to (19) to ensure that on average the scatterer power is equal to the thermal noise level, i.e., $\mathcal{E}\left\{\sigma_x^2 | \beta_0, \beta_1\right\} = K\bar{M}\sigma^2$, while allowing a large deviation from this value (see Fig. 4(b)).

B. Results

Performance of the Bayesian estimators (22) is illustrated hereafter and compared to the one obtained with the coherent integration defined by [3]

$$\left(\boldsymbol{a}^H \boldsymbol{y}\right) / \|\boldsymbol{a}\|_2^2. \tag{24}$$

Fig. 3 shows the range-velocity maps obtained with the different algorithms. As can be seen, the coherent integration (24) does not give a proper analysis of the radar signal. In particular, the signal amplitudes are not estimated accurately with this method. Furthermore, sidelobes present at ambiguous velocities are very high as expected and prevent from a correct identification of the scatterers. The MAP and MMSE estimators (22) give actually a sparse representation of the radar signal. Relative amplitudes are well restituted. Only a small amount of non-zero elements that do not correspond to a true scatterer are present on both maps. For the MMSE map, they are even not visible here[5].

Fig. 4 shows prior and empirical posterior PDFs for the parameters σ^2, w, σ_x^2. One can see that the histograms and MMSE estimates are in accordance with the scenario parameters even when flat prior distributions have been chosen (for σ^2 and w). Hence, the proposed Bayesian estimators (22) are able to use properly the range migration to alleviate the velocity ambiguity while giving an adequate sparse representation of the signal. Performances are satisfying even in a challenging scenario where range extended targets are hidden in the sidelobes of one another. Note that a very-low threshold would be required to remove false target detection. This threshold would be slightly higher for the MAP estimator. Finally, though computationally intensive, the Bayesian approach has the advantage to give further information such as an estimated value for the level of sparsity (contained in parameter w).

[5]The lowerbound of the colorbar has been set to the sixth-sidelobe level of the less powerful scatterers observed with (24) ($\approx f_0/(BM)/6$).

V. CONCLUSION

We have proposed a new Bayesian algorithm able to give an adequate sparse representation of multiple scatterer echoes for wideband LPRF radar waveforms. The method investigated in this work uses the additional information brought by the range migration to alleviate the velocity ambiguity with encouraging performance. The price to pay with the proposed method is its computational complexity which might be reduced using other MCMC methods or variational Bayes algorithms. Effects and robustification methods towards grid mismatches will be investigated in near future. Finally, to be implemented in real scenarios, the method ought to be further integrated in a wider detection scheme involving a clutter pre-filtering operation.

ACKNOWLEDGMENT

The authors would like to thank H. Rhzioual Berrada and A. Tamalet for the simulations conducted during their internship. They are also very grateful to F. Le Chevalier and O. Besson for many fruitful discussions about this work.

REFERENCES

[1] F. Le Chevalier, "Radar non ambigü à large bande," French Patent 9 608 509, 1996.

[2] N. Jiang, R. Wu, and J. Li, "Super resolution feature extraction of moving targets," *IEEE Trans. Aerosp. Electron. Syst.*, vol. 37, no. 3, pp. 781–793, July 2001.

[3] F. Le Chevalier, *Principles of Radar and Sonar Signal Processing*. Norwood, MA: Artech House, 2002.

[4] F. Deudon, S. Bidon, O. Besson, and J.-Y. Tourneret, "Spectral estimation of migrating targets in wideband radar," in *IEEE Int. Conf. on Digital Signal Processing*, Corfu, Greece, July6–8, 2011.

[5] S. Bidon, L. Savy, and F. Deudon, "Fast coherent integration for migrating targets with velocity ambiguity," in *IEEE Radar Conf. 2011*, Kansas City, Missouri, May 23–27, 2011.

[6] C. E. Shannon, "Communications in the presence of noise," *Proc. IRE*, vol. 37, pp. 10–21, Jan. 1949.

[7] J. Li and P. Stoica, "An adaptive filtering approach to spectral estimation and SAR imaging," vol. 44, no. 6, pp. 1469–1484, June 1996.

[8] R. Gribonval, "Should penalized least squares regression be interpreted as Maximum A Posteriori estimation?" *IEEE Transactions on Signal Processing*, vol. 59, no. 5, pp. 2405–2410, May 2011, to appear in IEEE Transactions on Signal Processing.

[9] S. Kay, *Fundamentals of Statistical Signal Processing : Estimation Theory*. Englewood Cliffs, NJ: Prentice Hall, 1993.

[10] N. Dobigeon, A. O. Hero, and J.-Y. Tourneret, "Hierarchical Bayesian sparse image reconstruction with application to MRFM," *IEEE Trans. Image Processing*, vol. 18, no. 9, pp. 2059–2070, Sept. 2009.

[11] M. I. Skolnik, *Radar Handbook*. McGraw-Hill, 1970.

[12] S. J. Godsill and P. J. W. Rayner, "Statistical reconstruction and analysis of autoregressive signals in impulsive noise using the gibbs sampler," *IEEE Trans. Speech Audio Processing*, vol. 6, no. 4, pp. 352–372, July 1998.

[13] C. P. Robert and G. Casella, *Monte Carlo Statistical Methods (Springer Texts in Statistics)*. Springer, 2004.

[14] H. Rhzioual Berrada, "Représentation parcimonieuse de signaux pour radar large bande," University of Toulouse/ ISAE-ENSEEIHT, Tech. Rep., 2010.

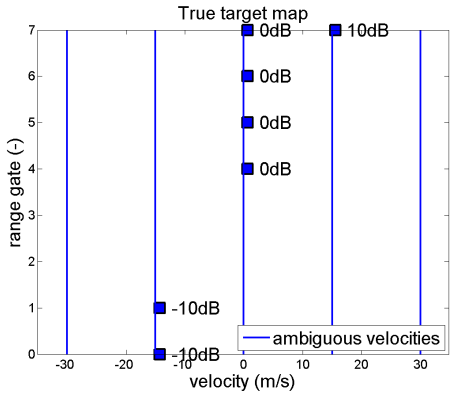

(a)

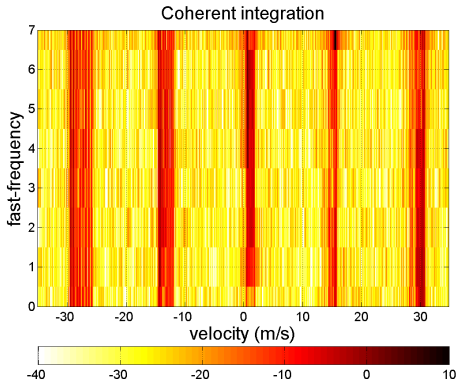

(b)

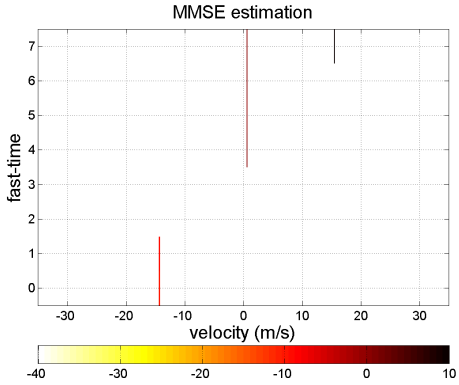

(c)

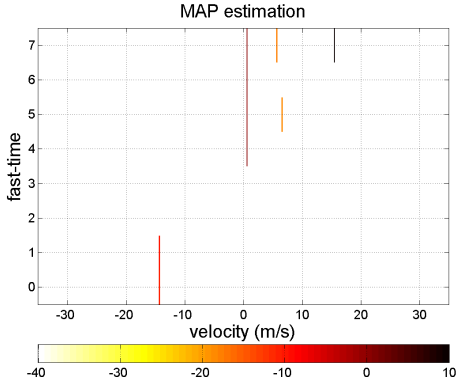

(d)

Fig. 3. Range-velocity map (amplitude only, in decibels). (a) True target map. (b) Coherent integration. (c) MMSE estimation. (d) MAP estimation.

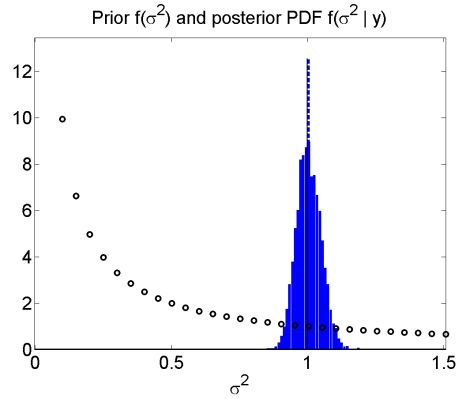

(a)

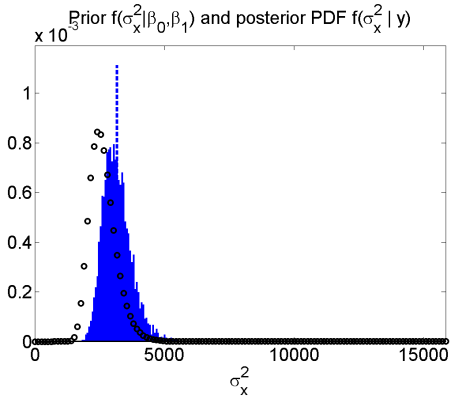

(b)

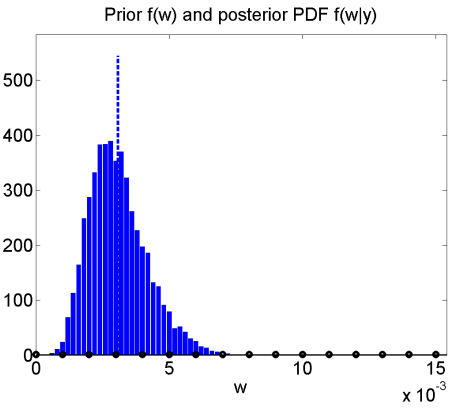

(c)

Fig. 4. Prior and empirical posterior PDFs. The circle markers represent the prior PDFs. The dashed lines represent the MMSE estimates. (a) Prior and posterior PDF of σ^2. The plain line represents the true value for σ^2. (b) Prior and posterior PDF of σ_x^2. (c) Prior and posterior PDF of w.